Atomistic Modeling of Pd Site Preference in NiTi

Guillermo Bozzolo[a,b,*], Ronald D. Noebe[b] and Hugo O. Mosca[c]

[a] *Ohio Aerospace Institute, 22800 Cedar Point Rd., Cleveland, OH 44142, USA*

[b] *NASA Glenn Research Center, Cleveland, OH 44135, USA*

[c] *Comisión Nacional de Energía Atómica, UAM, Av. Gral. Paz 1499, (B1650KNA) San Martín, Pcia. de Bs. As. Argentina*

Abstract

An analysis of the site substitution behavior of Pd in NiTi was performed using the BFS method for alloys. Through a combination of Monte Carlo simulations and detailed atom-by-atom energetic analyses of various computational cells, representing compositions of NiTi with up to 10 at% Pd, a detailed understanding of the site occupancy of Pd in NiTi was revealed. Pd substituted at the expense of Ni in a NiTi alloy will prefer the Ni-sites. Pd substituted at the expense of Ti shows a very weak preference for Ti-sites that diminishes as the amount of Pd in the alloy increases and as the temperature increases.

Keywords: Computer Simulations; Nickel; Titanium; Palladium; Shape Memory alloy; Semi-empirical methods; NiTi

1. Introduction

Binary NiTi alloys are technologically significant and commercially important materials utilized for their shape memory and superelastic properties for numerous applications around room temperature [1]. When alloyed with Pd, Pt, Au, Hf or Zr, NiTi also forms a family of alloys with great potential for use as high temperature shape memory materials [2].

Detailed knowledge of the site substitution behavior of these and other alloying additions is critical to the design of shape memory alloys with appropriate transformation temperatures and properties for specific applications. This information could also have substantial impact on our understanding of the martensitic transformation process in multicomponent alloys. In spite of the relevance of this topic, relatively few experimental or theoretical studies have been performed to

* Corresponding author: NASA Glenn Research Center, M. S. 23-2, Cleveland, OH 44135, USA. Tel: +1-216-4335824; Fax: +1-216-4335170. Guillermo.H.Bozzolo@grc.nasa.gov

determine the site preference behavior of ternary additions to NiTi.

Hosoda et al. [3] determined the general site preference of ternary additions in NiTi using pseudo-ground state analysis based on the nearest-neighbor pair approximation. The determination was made based on the magnitude of the energy of formation, establishing three zones in a ΔH_{NiX} vs. ΔH_{TiX} plot corresponding to absolute preference for Ni or Ti sites, regardless of alloy concentration, and an 'either-site' zone for elements that occupy available sites. Absolute site preference for Ni sites was found for Pd.

In spite of its basic similarity to the approach of Hosoda et al., a different behavior was found by Sheng et al. [4]. Based on electronic structure calculations using the discrete variational-X_α cluster method, the bond order B_{kl} between atoms k and l was computed in a cluster centered on atom X, the alloying addition, and two layers of neighboring atoms. The bond order is supposed to indicate the increase in electron density between the atoms due to bonding effects, thus giving a measure of the strength of the bond. If an alloying atom has a larger bond order with surrounding atoms on one lattice site, it forms stronger chemical bonds, thus lowering the total energy of the cluster, which is assumed to be an indication of site preference. A B_{Ni} vs. B_{Ti} plot (between X and the surrounding atoms when X occupies Ni and Ti sites, respectively) determines three regions by means of a 'Ni-subline' and a 'Ti-subline' passing through the points of Ni and Ti, respectively (B = 1). If the point is above the Ni-subline, the X atom forms a stronger bond with the surrounding atoms, making the cluster more stable, irrespective of the Ni:Ti ratio. Similarly, below the Ti-subline, X exclusively prefers Ti sites. The site preference in the intermediate region depends on stoichiometry. For example, their results show Pd and Pt in the intermediate region, close to the Ni subline, indicating that in a stoichiometric compound, Pd and Pt will prefer Ni sites. In a non-stoichiometric compound, Pd and Pt will take the sites of the insufficient element first, and then be distributed according to which line is nearer.

These results can be compared with ALCHEMI experiments [5] showing that the fraction of Pd atoms in Ni sites (for alloys with 5 at% Pd) is approximately 90%, regardless of whether Pd was added at the expense of Ni, Ti, or equally for both constituents. This would indicate a strong preference for Ni sites, regardless of the composition for dilute NiTiPd alloys, consistent with the results of Hosoda et al. [3]. However, given that even the slightest deviations in stoichiometry for $(Ni,Pd)_{50}Ti_{50}$ results in precipitation of second phases [6], it is not clear what the actual composition of the actual matrix material analyzed by Tadaki et al [5] would have been in their study of

site occupancy in NiTiPd alloys. It is doubtful that it was the same as their aim compositions.

The accuracy of analytical approaches can only be determined by confronting the theoretical predictions with experimental evidence, which in the particular case of NiTi, is extremely limited and open to interpretation due to the complexity of the microstructures. It is reasonable to expect that sound theoretical models could provide accurate and reliable information in most cases. But it is important to investigate the modeling efforts further, in order to fully understand the ramifications of the assumptions made within the idealized calculational schemes when comparing the modeled results with the reality of experiment, where such idealization is rarely achievable.

In this article we concentrate on the behavior of Pd additions to NiTi, in significantly more detail than previously performed, by means of a modeling effort using the BFS method for alloys [7], a quantum approximate method with a good track record of success in describing the fundamental energetics of multicomponent systems [8-10]. While zero temperature calculations are performed in order to understand the detailed energetics of Pd additions to NiTi over a broad range of concentrations, temperature dependent effects are introduced through Monte Carlo simulations.

2. The BFS method for alloys

The BFS method for alloys [7] is based on the concept that the energy of formation of a given atomic configuration is the sum of the individual atomic contributions, $\Delta H = \Sigma \varepsilon_i$. Furthermore, each contribution by atom i, ε_i, can be calculated as the sum of two terms: a strain energy, ε_i^S, computed in the actual lattice as if every neighbor of the atom i were of the same atomic species i, and a chemical energy, ε_i^C, computed as if every neighbor of the atom i were in an equilibrium lattice site of a crystal of species i, but retaining its actual chemical identity.

The computation of ε_i^S, using Equivalent Crystal Theory (ECT) [11], involves three pure element properties for atoms of species i: cohesive energy, lattice parameter and bulk modulus. These three parameters for each of the constituent elements are needed in the general derivative structure as the final alloy. Consequently, when studying bcc-based alloys such as the B2-structured NiTi, the elements would need to be parameterized as if they were A2 (bcc).

The chemical energy, ε_i^C, accounts for the corresponding change in composition, considered as a defect in an otherwise pure crystal. The chemical 'defect' deals with pure and mixed bonds,

therefore, two additional perturbative parameters (Δ_{AB} and Δ_{BA} where A, B = Ni, Ti, Pd) are needed to describe these interactions. A reference chemical energy, ε_i^{Co}, is also included to insure a complete decoupling of structural and chemical features. All the needed BFS parameters are determined with the Linearized-Augmented Plane Wave method (LAPW) [12]. Finally, the strain and chemical energies are linked with a coupling function g_i, which ensures the correct volume dependence of the BFS chemical energy contribution. Therefore, the contribution of atom i to the energy of formation of the system is given by

$$\varepsilon_i = \varepsilon_i^S + g_i(\varepsilon_i^C - \varepsilon_i^{C_0}) \quad (1)$$

Table 1 lists the necessary parameters for applying the BFS method to the Ni-Ti-Pd system. As with any other quantum approximate method relying on first-principles parameterization, all LAPW-generated parameters are the result of zero temperature calculations. Finite temperature enters the current formalism only via Monte Carlo simulations. Additional analytical calculations for the determination of the absolute site preference are performed exclusively at zero temperature. In spite of the limitation of using parameters that do not depend on temperature, finite-temperature properties can be accurately reproduced as shown, for example, in recent calculations using BFS and Monte Carlo simulations for the determination of the coefficient of lattice expansion of multi-component superalloys [13] and the order-disorder transitions in Cu-Pd alloys [14]. We refer the reader to Ref. 7 for detailed discussions of the BFS method, its definitions, operational equations and their implementation.

3. Results

In this section we examine the site substitution behavior from two different perspectives. First, we perform an energy analysis of the possible substitutional schemes with varying Pd concentration, supplemented with an atom-by-atom analysis of the energetics in each case. In doing so, we can determine absolute site preference, as has been performed in a number of previous applications of BFS [8-10]. This past approach, however, is incomplete, as it is based on a number of assumptions that are not necessarily valid when analyzing for site occupancy under experimental conditions. On the other hand, and in spite of its potential limitations, modeling can provide information that would otherwise be impossible to extract from one single experimental case.

We perform this type of analysis in several steps. First, we consider the case of a single Pd atom in a (Ni,Pd)Ti or a Ni(Ti,Pd) alloy, from which zero temperature absolute site preference can be determined. Second, we extend this analysis to the case of additional Pd atoms, identifying interactions that are not immediately apparent from the limited case of a single solute atom. To verify these trends and in order to visualize their effect in situations that better resemble experimental conditions including finite temperature, the second part of this section deals with the analysis of large scale Monte Carlo simulations. By combining these two methods we can provide a more complete picture of the behavior of Pd in NiTi. Correlation of the zero temperature "static" energy calculations, with Monte Carlo simulations, indicates how preferred behaviors manifest themselves under more realistic conditions and therefore, more in line with experimental expectations. Large scale simulations of the annealing of different NiTiPd alloys, using traditional Monte Carlo - Metropolis exchange algorithms (MCAS) [9] provide information regarding the thermodynamical ground state of the system. However, experimental results still usually differ from such ideal states. In this paper, we also implement a variant of the traditional Monte Carlo - Metropolis algorithm which, although approximate in nature, provides a better modeling framework for diffusion processes, thus leading to final states that are more appropriate for comparison with experiment. Known as the BANN algorithm [9], atoms of different species are allowed to exchange with only nearest-neighbor (NN) sites until an equilibrium state is reached at each temperature. The exchanges are accepted or rejected in terms of a probabilistic factor which depends on the available thermal energy [9]. In this way, it is possible for atoms to "lock" themselves into metastable configurations that may be slightly higher in energy than that found using the MCAS method, which allows atoms to swap *any* two positions in the computational cell until the lowest energy configuration is found. In either technique, the initial state consists of Ni, Ti and Pd atoms randomly situated in the computational cell. All the simulations in this paper used 1024 atom cells and in all cases the initial state (representing the high temperature disordered state) consists of a random distribution of the appropriate number of Ni, Ti and Pd atoms. The temperature cycle in both MCAS and BANN simulations is a monotonous decrease in temperature, ending at T = 1 K. At each temperature stage, the cell is allowed to equilibrate (i.e., no further changes in the energy of formation after a sufficiently large number of exchanges).

It should be noted that the simulations are performed in rigid bcc lattices, only allowed to isotropically expand or contract in order to optimize the value of the lattice parameter at each tem-

perature. The low temperature MCAS results assume that the system will retain a bcc symmetry and not undergo a martensitic transformation. Based on experimental data [1], this is clearly not correct, but due to the character of these diffusionless transformations, no changes in site preference behavior would be expected. The martensite phase would retain the basic order of the parent B2 phase. Therefore, we have included these results primarily to show the ordering tendencies of the B2 phase as a function of temperature. In the BANN case, however, equilibrium is reached at rather high temperatures, making it unnecessary to distinguish between high and low temperature regimes.

Throughout this work, we introduce a notation that is equally convenient for simple or complex configurations. If A and B represent the two simple cubic sublattices of the B2 compound, P(A) denotes a Pd atom substituting for an atom A on the A sublattice. If the displaced A atom goes on to occupy a site in the B sublattice (A(B)), the two defects can be connected by denoting them as $Pd(A)A(B)_d$. In this case, the subindex d distinguishes between the pair of defects (Pd(A) and A(B)) being nearest neighbors (d = 1), next-nearest neighbors (NNN) (d = 2), or the pair being separated by distances greater than that (either no subindex or $d = f$).

The determination of the site preference of Pd in NiTi involves asking the following questions. The first, basic question, refers to the absolute site preference. Consider, for example, a (Ni,Pd)Ti alloy and a site available in the Ni sublattice. Does Pd necessarily prefer that site (Pd(Ni)) or does it go to a site in the Ti sublattice, Pd(Ti), creating an antistructure Ti atom, Ti(Ni), in the process? To answer this, we compare the energy of formation of the different configurations possible for a Pd atom in a NiTi cell, shown in Fig. 1. For a $Ni_{50}(Ti,Pd)_{50}$ alloy, Figs. 1.a-c show the Pd atom a) occupying a Ti-site, Pd(Ti), b) displacing a Ni atom to a Ti-site at NN distance, $Pd(Ni)Ni(Ti)_1$, or c) farther away, $Pd(Ni)Ni(Ti)_f$. For a $(Ni,Pd)_{50}Ti_{50}$ alloy, Figs. 1.d-f show the Pd atom d) occupying a Ni-site, Pd(Ni), e) displacing a Ti atom to a Ni-site at NN distance, $Pd(Ti)Ti(Ni)_1$, or f) farther away, $Pd(Ti)Ti(Ni)_f$. These results indicate preference for the available sites: Pd(Ti) in $Ni_{50}(Ti,Pd)_{50}$ and Pd(Ni) in $(Ni,Pd)_{50}Ti_{50}$. The zero temperature energy gap between the lowest energy state and the next energy state is noticeably different in each case. There is only a 0.001 eV gap between Pd(Ti) and Pd(Ni)Ni(Ti) in $Ni_{50}(Ti,Pd)_{50}$ alloys and a 0.008 eV gap between Pd(Ni) and Pd(Ti)Ti(Ni) in $(Ni,Pd)_{50}Ti_{50}$ alloys. This could be viewed as a definite preference for Ni sites in (Ni,Pd)Ti alloys and a less defined preference for Ti sites in Ni(Ti,Pd) alloys. However, the small energy gap in Ni(Ti,Pd) alloys raises the question of whether composition, temperature, or

kinetics could alter the preferred site preference scheme in the alloys where Pd substitutes for Ti, eventually favoring Ni sites, as would be supported by the argument that the strong binding energy of TiPd alloys [11] would favor Pd atoms in Ni sites in spite of their absolute preference for Ti sites.

Besides the absolute site preference (as determined by the energy gap between direct substitutions, Pd(X), against the creation of antisite defects, Pd(Y)Y(X), a related question must be simultaneously addressed: what are the energetics of Pd in either site (regardless of the existence and/or location of an antistructure atom)? This is important because atoms could eventually get 'trapped' in unfavorable sites, and whether they do or not could be a consequence of the interplay of the alloying addition, in this case Pd, with its local environment. Therefore, we concentrate on the atom-by-atom energetics of the local environment surrounding direct Pd(Ni) and Pd(Ti) substitutions (i.e., the Pd atom and its shells of NN and NNN). Opposite behaviors describe each situation. Table 2 shows the BFS contributions to the total energy of formation for a 15 atom cluster (embedded in a NiTi cell) with the Pd atom at the center of the cluster, its 8 NN and 6 NNN. To understand the effect of replacing either a Ti or a Ni atom with Pd, the values of E(total) in Table 2 should be compared to the 'original' values that a Ti or a Ni atom would contribute in a pure NiTi B2 cell: +2.7153 eV for Ni, and -3.4176 eV for Ti. The last column in Table 2 displays the net changes in energy for the Pd atom, its eight NNs, and six NNNs, as well as the overall energy gain (lower energy of formation) or loss (higher energy of formation) relative to a pure NiTi cluster. These results indicate that replacing a Ti atom with a Pd atom lowers the energy of formation of the cluster by 0.5556 eV. This configuration is favorable for the surrounding Ni NNs and Ti NNNs created, offsetting an energy loss by Pd(Ti). This could be understood as if the Pd(Ti) atom is energetically locked into place by its surrounding Ni and Ti atoms. Conversely, Table 2 shows that the Pd(Ni) atom sits comfortably in the Ni site, in spite of the unfavorable effect on the surrounding Ti NNs. Figuratively, in terms of BFS language, one can look at this as if the Pd(Ni) attracts the 8 Ti NN around it, whereas Pd(Ti) is locked into a unfavorable site by the surrounding 8 Ni NN.

Additional detail on the evolution of the energetics of these substitutional defects can be obtained by adding another Pd atom in the computational cells. This was done by creating "catalogs" of atomic configurations dealing with all the possible combinations of two Pd atoms in an otherwise equilibrium NiTi cell (a = 3.0150 Å). The three main substitutional schemes are: a)

$Ni_{50}Ti_{50-x}Pd_x$ alloys: Pd can occupy an available Ti site [Pd(Ti)] or go to a Ni site displacing the Ni atom to a the available Ti site [Pd(Ni)Ni(Ti)]. The two possible locations of the displaced Ni atom should be considered: when Ni(Ti) remains close to Pd(Ni) [$Pd(Ni)Ni(Ti)_1$] and when it migrates somewhere else in the lattice [$Pd(Ni)Ni(Ti)_f$]. b) $Ni_{50-x}Ti_{50}Pd_x$ alloys: Pd can occupy an available Ni site [Pd(Ni)] or go to a Ti site displacing the Ti atom to the available Ni site [Pd(Ti)Ti(Ni)]. Two possibilities should be considered: when Ti(Ni) remains close to Pd(Ti) [$Pd(Ti)Ti(Ni)_1$] and when it migrates somewhere else in the lattice [$Pd(Ti)Ti(Ni)_f$]. c) $Ni_{50-x/2}Ti_{50-x/2}Pd_x$ alloys: a combination of the previous two cases.

Table 3 shows the energies of formation of rigid cells in all these possible configurations. In each substitution scheme, lower energies of formation are obtained with direct substitutions (i.e., no antisite atoms). For Ni(Ti,Pd) alloys, the energy spread between the lowest energy state (two isolated Pd(Ti) atoms) and the highest (a tight cluster of Pd(Ni)Ni(Ti) substitutions) is less than 3 eV, indicating that all type of substitution schemes are almost equally possible. The spread widens for equiatomic (Ni,Pd)(Ti,Pd) alloys, and grows to nearly 20 eV for (Ni,Pd)Ti alloys, thus favoring direct Pd(Ni) substitutions by a wide margin. Fig. 2 shows the three energy level spectra for the cases displayed in Table 3, including intermediate states that differ in the distance between the various defects (note the expanded scale between the three cases).

To study the atom-by-atom energy contributions for the two Pd atoms case, a specific configuration, chosen to examine the effect of proximity between the Pd atoms was compared to a NiTi cell. The results are listed in Table 4. The case of two Pd(Ti) atoms in NNN sites lower the energy of formation of the cell by 0.9308 eV. This is a reduction, per Pd(Ti) atom, from 0.5556 eV in the single Pd atom case to 0.4654 eV). Conversely, two Pd(Ni) atoms in NNN sites raise the energy of formation by 1.1808 eV. This is a reduction, per Pd(Ni) atom, from 0.6688 eV in the single Pd atoms case to 0.5904 eV. Overall, the Pd(Ti) substitutions become less favorable and the Pd(Ni) substitutions become more favorable, suggesting that increasing Pd concentration could lead to a reversal of site preference in experimental situations.

The case of one and two Pd atoms suggest that the above mentioned 'reversal' might continue with subsequent Pd additions. The case with four Pd atoms continues this trend. The comparison of a square Pd(Ti) patch with a similar Pd(Ni) case, results in further reductions of gains and losses (per atom) in each case: 0.3597 eV for Pd(Ti) and 0.4878 eV for Pd(Ni). The atom-by-atom analysis of these cases are shown in Table 5. While the absolute site preference scheme does not

change (Pd still prefers Ti sites in Ni(Ti,Pd) alloys and Ni sites in (Ni,Pd)Ti alloys), the trend seen with increasing Pd concentration indicates that the already small energy gap favoring Pd(Ti) substitutions becomes less relevant, thus increasing the chances of finding Pd(Ni)Ni(Ti) defects (Pd in Ni sites with Ni antistructure atoms in Ti sites).

The eight Pd atom case provides additional evidence on how the substitutional process takes place, indicating the relevant role of a possible TiPd environment within the NiTi matrix. Table 6 shows the energy level spectra of a catalog of numerous 8Pd configurations in a) Ni(Ti,Pd) and b) (Ni,Pd)Ti alloys, displayed in Fig. 3. Two opposite trends emerge: Pd(Ni) atoms tend to coalesce forming a B2 TiPd 'bubble' while Pd(Ti) atoms balance repulsion and attraction resulting in a 2x2 ordered pattern [13].

4. BANN and MCAS simulations

As noted in the previous section, the slight absolute preference of Pd for Ti sites in Ni(Ti,Pd) alloys is further diminished with increasing Pd concentration. As seen above, the energy gap between Pd(Ti) and Pd(Ni) substitutions decreases, due to the formation of TiPd bonds when Pd goes to otherwise unfavorable Ni sites. It appears then that when and if Pd atoms substitute for Ni sites, they have a strong likelihood to remain in those sites. To show this, the following describes the results of BANN and MCAS long simulations of 1024 atom cells with decreasing temperatures. At each temperature the cell is allowed to equilibrate (i.e., no changes in the energy of formation).

$Ni_{50}(Ti,Pd)_{50}$ alloys: these alloys should be characterized by direct Pd(Ti) substitutions. However, this is not generally the case:

a) $Ni_{50}Ti_{49}Pd_1$: BANN (Fig. 4.a) ultimately evolves towards a stable B2 structure where 70% of the Pd atoms go to Ni sites in spite of their weak absolute preference for Ti sites, creating Ni(Ti) antistructure atoms. The remaining 30% perform direct substitutions for Ti sites. During MCAS simulations (Fig. 5.a) with a similar temperature cycle, the NiTi matrix orders at high temperature (HT) with 80% of the Pd atoms in Ni sites. At low temperatures (LT) the system stabilizes with all the Pd atoms in Ti sites. There is an additional change at extremely low temperatures (between 1 and 100 K), where the Pd(Ti) atoms establish an ordered pattern. It is remarkable that the energies of the random distribution of Pd(Ti) atoms and the ordered T = 1 K state differ only

by 0.1 eV. As mentioned before, however, the formation of this ordered structure at LT is somewhat unrealistic, given that the system is expected to undergo a martensitic transformation before reaching this temperature range. These results, however, indicate that there is a latent trend for ordering which can not be readily extracted from experimental results at room temperature or above.

b) $Ni_{50}Ti_{45}Pd_5$: BANN simulations (Fig. 4.b) show similar features as the previous case, where the system equilibrates with 25% Pd(Ni)Ni(Ti) and 75% Pd(Ti) atoms. MCAS simulations (Fig. 5.b) behave similarly. After a HT state with an almost equal number of randomly located Pd(Ni)Ni(Ti) and Pd(Ti) atoms, all Pd atoms substitute for Ti sites as the temperature decreases. Once again, there is further ordering at extremely low temperatures, where the Pd(Ti) atoms order in a 2x2 pattern (Pd(Ti) atoms are separated by Ti atoms along the [001] and [010] directions). It should be noted that the 2x2 pattern may not necessarily represent a real precipitate phase. Within the context of the present model calculation, where interactions between atoms up to NNN distance are considered, Ti atoms barely "connect" otherwise noninteracting Pd(Ti) atoms thus leading to this long-range order scheme. It could be possible that longer range interactions might lead to other alternative arrangements which might ultimately lead to order or Pd atoms in solution in the Ti sublattice. This is clear from the calculations, which predict an extremely small difference in energy of formation (0.7 eV) between the 2x2 and Pd(Ti) disordered state.

c) $Ni_{50}Ti_{40}Pd_{10}$: BANN (Fig. 4.c) displays an almost continuous drop down to 1000 K where an initial, almost even, distribution of Pd(Ni)Ni(Ti) and Pd(Ti) atoms, evolves into a 10% Pd(Ni)Ni(Ti) state. MCAS (Fig. 5.c) results again display a HT metastable state characterized by an even number of Pd(Ni)Ni(Ti) and Pd(Ti) atoms, and a low temperature state stabilizing in what appears to be a mixture of $L2_1$ and 2x2 ternary phases. Once again, the lowest energy state for T = 1 K is a 2x2 ordered phase.

(Ni,Pd)Ti alloys automatically favor Pd(Ni) substitutions. However, additional features emerge from BANN and MCAS simulations:

a) $Ni_{49}Ti_{50}Pd_1$: BANN (Fig. 6.a) results display a steady drop of energy of formation towards a steady state with 80% of Pd(Ni) substitutions and 20% Pd(Ti)Ti(Ni). The MCAS simulation (Fig. 7.a) stabilizes in a HT state characterized by a random distribution of Pd(Ni) atoms, and a LT state where after a small reduction in energy of formation, of only 3 eV, yields a B2 TiPd precipitate.

b) $Ni_{45}Ti_{50}Pd_5$: During the BANN (Fig. 6.b) simulation, there is a steady drop in energy due to the loss of Pd(Ti)Ti(Ni) atoms until the system settles in a stable cell with only Pd(Ni) substitutions. Once again there is a double drop in the MCAS (Fig. 7.b) simulation, first settling into a NiTi cell with a random distribution of Pd(Ni) atoms, evolving into a TiPd B2 precipitate at lower temperatures.

c) $Ni_{40}Ti_{50}Pd_{10}$: Similar to the previous two cases, the BANN (Fig. 6.c) simulation shows a continuous decrease in energy corresponding to a decrease in the number of Pd(Ti)Ti(Ni) atoms. The sample stabilizes at 800 K, with just a few Pd(Ti)Ti(Ni) atoms left. The MCAS (Fig. 7.c) simulation once again displays a HT and LT metastable states that monotonically evolve to a two-phase NiTi/TiPd alloy.

Lastly, for equiatomic NiTi alloys, equal number of direct substitutions should be expected, but the results seem to depend on Pd concentration:

a) $Ni_{49}Ti_{49}Pd_2$: The BANN simulation (Fig. 8.a) evolves into a state where 75% Pd atoms reside in Ni sites and only 25% in Ti sites, with no specific order. The MCAS (Fig. 9.a) simulation shows a three-step decay: the high temperature states are characterized by 90% Pd(Ni) atoms, well in excess of the expected 50%. A second drop leads to a B2 cell with a TiPd precipitate and some additional Pd(Ti) random atoms. It is only at very low temperatures (100K-1K) when the system evolves to a three phase alloy, where the random Pd(Ti) atoms order in a 2x2 phase.

b) $Ni_{45}Ti_{45}Pd_{10}$: The BANN simulation (Fig. 8.b) evolves into a state with equal number of Pd(Ni) and Pd(Ti) atoms, while the MCAS simulation (Fig. 9.b) evolves into a three phase alloy, that is clearly distinguished only at extremely low temperatures. The three phase alloy consists of B2 TiPd, B2 NiTi, and a 2x2 phase.

5. Discussion and Conclusions

Absolute site preference calculations indicate that Pd will go to the available site in NiTi alloys. In Ni(Ti,Pd) alloys, it will go to Ti sites and in (Ni,Pd)Ti alloys, to the Ni sublattice. One measure of this preference (beyond the determination of the configuration with the lowest energy) is the energy gap between the direct substitution Pd(X) and the creation of an antistructure atom in order to allow for the opposite choice. This gap is substantial in a (Ni,Pd)Ti alloy, guaranteeing preference for Ni sites. It is nearly negligible in Ni(Ti,Pd) alloys, thus making it more likely that

Pd will substitute for Ni, even at the expense of creating a Ni(Ti) antistructure atom.

BANN simulations, which tend to give a more realistic description of the simulated annealing process, indicate that in almost every Ni(Ti,Pd) alloy, a large fraction of Pd atoms go to Ni sites and stay there, in spite of the fact that Pd(Ti) substitutions would be, in principle, favored. In all cases, even at low temperatures, the final state of the cell is a basically a NiTi B2 structure with scattered Pd(Ti) atoms and some Pd(Ni)Ni(Ti) defects. MCAS simulations, on the other hand, do not show this behavior. While some Pd(Ni)Ni(Ti) defects exist at high temperatures, they are eliminated at low temperatures and eventually the system evolves to an ordered Ni(Ti,Pd) alloy (either an $L2_1$ or a 2x2 precipitate). The substantial contrast between BANN simulations (leading to a B2 phase) and MCAS simulations (leading to Ni_2TiPd or Ni_4Ti_3Pd precipitates) indicates that kinetics are very important and that there are important differences between the energetics of Pd(Ti) and Pd(Ni) substitutions (regardless of the formation of Ni(Ti) atoms in the second case).

The atom-by-atom calculations shown in Tables 2, 4 and 5 indicate that there are two distinct behaviors. When a Pd atom moves to a Ni site, the energetics of the local environment indicate that Pd benefits from such substitution, attracting the first layer of Ti neighbors around it. Even if there was a better configuration requiring the rearrangement of the local environment, a Pd(Ni) atom would tend to choose to remain there. On the other hand, the 'direct substitution' (Pd(Ti)) introduces a gain in energy mostly due to the atoms in the local environment rather than Pd. It could be thought of as if Pd(Ti) is energetically favorable because the benefit for the surrounding Ni and Pd atoms.

Increasing the number of neighboring Pd atoms shows that this basic difference between Pd(Ni) and Pd(Ti) substitutions has further consequences. If two Pd atoms occupy neighboring Ni sites, the preference is improved (less energy loss per atom than in the single atom case), thus making it more favorable that Pd(Ni) atoms will coalesce in otherwise unfavorable sites. Conversely, increasing the number of neighboring Pd(Ti) direct substitutions decreases the energy gain, leading to a 'repulsion' of Pd(Ti) atoms (as isolated Pd(Ti) substitutions would be more favorable). This was clearly illustrated in Table 4 for two Pd atoms. In the case of four Pd atoms, this trend continues but a new trend appears: the coalescence of Pd(Ni) atoms leads to the formation of a TiPd precipitate.

It can be concluded then that the substitution of Pd for Ni sites in Ni(Ti,Pd) alloys, while less favorable than Pd(Ti) substitutions in absolute terms, would be highly achievable during the pro-

cess of alloy formation due to the consequences of the detailed atom-by-atom energy balance. These factors, which include the interplay of Pd in different environments, the effect of diffusion, Pd concentration, temperature treatment, etc., and their role in the determination of the site preference behavior, are not immediately apparent from the straightforward analysis of Pd(Ni)Ni(Ti) vs. Pd(Ti) defects. A clear example of this is the exceedingly small nature of the predicted difference in energy of formation of the B2 cell (observed experimentally) and the exact thermodynamical ground state (ordered Heusler/2x2 precipitate), averaging less than 0.001 eV per atom.

Acknowledgements

Fruitful discussions with N. Bozzolo are gratefully acknowledged. This work was sponsored by the Alternate Fuel Foundation Technologies Subproject of the Low Emissions Alternative Power Project at the NASA Glenn Research Center, Cleveland, Ohio.

References

1. P. G. Lindquist and C. M. Wayman, in Engineering Aspects of Shape Memory Alloys, eds. T. W. Duerig, K. N. Melton, D. Stockel and C. M. Wayman, Butterworth-Heinemann, London, (1990) pp. 58-68.
2. J. Van Humbeeck, Trans. ASME, 121 (1999) 98.
3. H. Hosoda, A. Kamio, T. Suzuki and Y. Mishima, J. Japan Inst. Metals 60 (1996) 793.
4. X. D. Sheng, S. Yan, L. Dong and H. Z. Qi, Phil. Mag. A75 (1997) 1185.
5. T. Tadaki, Y. Nakata and K. Shimizu, J. de Physique IV, 5 (1995) 81.
6. S. Shimizu, Y. Xu, E. Okunishi, S. Tanaka, K. Otsuka, K. Mitose, Mater. Letters 34 (1998) 23.
7. G. Bozzolo and J. E. Garcés, The Chemical Physics of Solid Surfaces, D. P. Woodruff ed., Elsevier, 2002, p. 30.
8. G. Bozzolo, H. Mosca, A. W. Wilson, R. D. Noebe and J. Garcés, Metall. Mater. Trans. B 33 (2002) 265.
9. G. Bozzolo, J. Khalil and R. D. Noebe, Comp. Mat. Sci. 24 (2002) 457.
10. G. Bozzolo, R. D. Noebe and C. Amador, Intermetallics 10 (2002) 149.
11. J. R. Smith, T. Perry, A. Banerjea, J. Ferrante and G. Bozzolo, Phys. Rev. B 44 (1991) 6444.

12. P. Blaha, K. Schwartz, J. Luitz, WIEN97, Vienna University of Technology. Updated Unix version of the copyrighted WIEN code, P. Blaha, P. Schwartz, P. Sorantin, S. B. Trickey, Comput. Phys. Commun. 59 (1990) 399.
13. Q. Guo and O. J. Kleppa, J. Alloys Comp. 266 (1998) 224.

Figure captions:

Fig. 1: Basic cell configurations used to determine the site preference of Pd in NiTi. The top row shows three possible locations for a Pd atom in a $Ni_{50}(Ti,Pd)_{50}$ alloy. The bottom row shows the corresponding cases in a $(Ni,Pd)_{50}Ti_{50}$ alloy. The energy of formation (in eV/atom) is indicated in each case. Ni and Ti atoms are represented with grey and open disks, respectively. The Pd atom is indicated with a black disk.

Fig. 2: Energy level spectra for two Pd atoms in a (a) Ni_{50}(Ti,Pd)50, (b) (Ni,Pd)(Ti,Pd), and (c) (Ni,Pd)Ti alloy, including the energy levels show in Table 3. The energy levels are grouped according to the type of defects included in the corresponding configurations.

Fig. 3: Configurations with 8 Pd atoms in a B2 cell (see Table 6).

Fig. 4: Final states of BANN simulations (300 K) of $Ni_{50}Ti_{(50-x)}Pd_x$ (x = 1, 5, 10 at%) alloys. Ni, Ti and Pd atoms are denoted with grey, white, and black spheres, respectively. No further changes are seen in the cell below room temperature.

Fig. 5: Final states of MCAS simulations (300 K and 1 K) of $Ni_{50}Ti_{(50-x)}Pd_x$ (x = 1, 5, 10 at%) alloys. Ni, Ti and Pd atoms are denoted with grey, white, and black spheres, respectively.

Fig. 6: Final states of BANN simulations (300 K) of $Ni_{(50-x)}Ti_{50}Pd_x$ (x = 1, 5, 10 at%) alloys. Ni, Ti and Pd atoms are denoted with grey, white, and black spheres, respectively. No further changes are seen in the cell below room temperature.

Fig. 7: Final states of MCAS simulations of $Ni_{(50-x)}Ti_{50}Pd_x$ (x = 1, 5, 10 at%) alloys. Ni, Ti and Pd atoms are denoted with grey, white, and black spheres, respectively.

Fig. 8: Final states of BANN simulations of $Ni_{(50-x/2)}Ti_{(50-x/2)}Pd_x$ (x = 2, 10 at%) alloys. Ni, Ti and Pd atoms are denoted with grey, white, and black spheres, respectively. No changes are seen in the computational cell between 300 K and 1 K.

Fig. 9: Final states of MCAS simulations (300 K and 1 K) of (Ni,Pd)(Ti,Pd) alloys. Ni, Ti and Pd atoms are denoted with grey, white, and black spheres, respectively.

Table captions:

Table 1: LAPW results for the lattice parameter, cohesive energy, and bulk modulus calculated for the bcc phases of Ni, Ti and Pd, the resulting equivalent crystal theory (ECT) parameters p, α, l and λ, and the BFS perturbative parameters Δ_{AB} and Δ_{BA}.

Table 2: Individual BFS contributions to the energy of formation (in eV/atom) of each non-equivalent atom in a Ni(Ti,Pd) alloy and a (Ni,Pd)Ti alloy. The last column shows the total change in energy (counting 8 NN and 6 NNN contributions) with respect to a NiTi cell. The total change in energy of formation due to the presence of the Pd atom is the direct sum of the last column energies (in eV/atom).

Table 3: Highest and lowest energy states for 2Pd atoms in a Ni(Ti,Pd), (Ni,Pd)(Ti,Pd), and (Ni,Pd)Ti for each type of defect present in the cell. The substitutional scheme is shown in the third column. In each diagram, the top line represents the Ti sublattice (open circles) and the bottom line the Ni sublattice (gray circles). Pd atoms are denoted with black disks. The last column lists the total energy of formation of the cell at the equilibrium lattice parameter of NiTi.

Table 4: Atom-by-atom analysis of (a) Pd(Ti)Pd$(Ti)_2$ and (b) Pd(Ni)Pd$(Ni)_2$. The multiplicity (M) is the number of equivalent atoms in the cell. The subindices denote the distance (in neighbor layers) between Ni (or Ti) and with each of the two Pd(Ni) (or Pd(Ti)) atoms. The last column dis-

plays the difference in individual contributions to the energy of formation (in eV/atom) of each atom and the original (Ni or Ti) atom in the B2 cell for (a) Ni(Ti,Pd) or (b) (Ni,Pd)Ti alloys.

Table 5: Atom-by-atom analysis of a four Pd atom forming a square in a (100) plane. The multiplicity (M) is the number of equivalent atoms in the cell. The subindices denote the distance (in neighbor layers) between surrounding Ni or Ti atoms and each of the four Pd(Ti) (or Pd(Ni)) atoms. The last column displays the difference in individual contributions to the energy of formation (in eV/atom) of each atom and the original (Ni or Ti) atom in the B2 cell for (a) Ni(Ti,Pd) or (b) (Ni,Pd)Ti alloys.

Table 6: Energy of formation and equilibrium lattice parameter of a set of configurations with different distributions of eight Pd atoms (see Fig. 3). Arranged from higher to lower (more stable) energy, the top entries correspond to eight Pd atoms in Ti sites in a Ni(Ti,Pd) alloy. The bottom entries refer to configurations with eight Pd atoms in Ni sites in a (Ni,Pd)Ti alloy.

Table 1
Parameters needed for performing BFS calculations of B2 NiTiPd alloys

	Lattice parameter	Cohesive energy	Bulk modulus	ECT parameters			
	(Å)	(eV)	(GPa)	p	$\alpha(Å^{-1})$	l(Å)	λ(Å)
Ni	2.7985	5.6001	198.29	6	3.05968	0.29494	0.82878
Ti	3.2552	5.7825	105.44	6	2.69236	0.38109	1.07085
Pd	3.1358	4.0148	172.45	8	3.48602	0.25297	0.71086
BFS parameters (in $Å^{-1}$)							
Δ_{NiTi}	-0.074001		Δ_{NiPd}	-0.021765		Δ_{TiPd}	+0.080218
Δ_{TiNi}	+0.481946		Δ_{PdNi}	-0.037241		Δ_{PdTi}	-0.064662

Table 2
Atom-by-atom energetics of a single Pd atom in a B2 NiTi cell

	Atom	E(strain) (eV/atom)	Glue	E(chemical) (eV/atom)	E(total) (eV/atom)	Net change with respect to NiTi (eV)
Pd(Ti)	Pd(Ti)	0.1299	1.2650	-0.1648	-0.0786	+3.3390
	Ni(NN)	0.2885	0.6967	2.8793	2.2944	-3.3672
	Ti(NNN)	0.3433	1.3639	-2.8220	-3.5055	-0.5274
						-0.5556
Pd(Ni)	Pd(Ni)	0.1230	1.2650	0.6080	0.8991	-1.8162
	Ti(NN)	0.3433	1.3639	-2.5290	-3.1058	+2.4944
	Ni(NNN)	0.2885	0.6967	3.4812	2.7138	-0.0090
						+0.6692

Table 3
Energy of formation of various NiTiPd alloys with different substitutional defects

Alloy	Type of defects	Description	ΔH (eV/atom)
$Ni_{50}Ti_{50-x}Pd_x$	Two antisite atoms	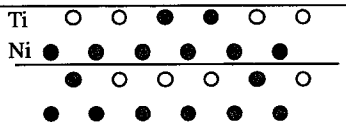	-0.34937 -0.34985
	One antisite atom	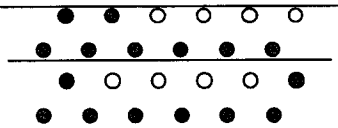	-0.35071 -0.35090
	Direct substitutions	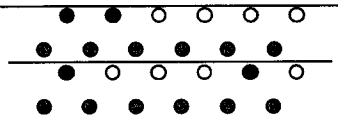	-0.35204 -0.35222
$Ni_{50-x/2}Ti_{50-x/2}Pd_x$	Two anti-site atoms	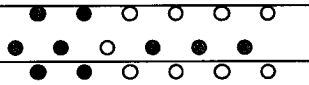	-0.34126
	One Ti(Ni) atom	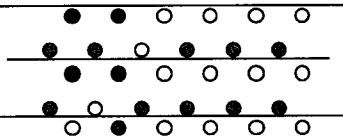	-0.34261 -0.34361
	One Ni(Ti) atom	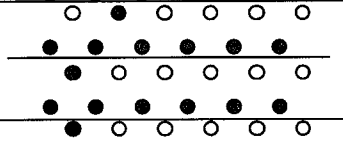	-0.34992 -0.34998
	Direct substitutions	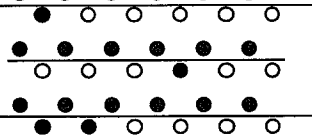	-0.35096 -0.35103
$Ni_{50-x}Ti_{50}Pd_x$	Two antisite atoms	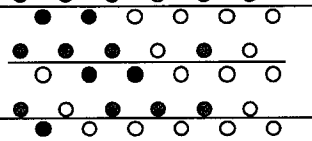	-0.33143 -0.33701
	One antisite atom	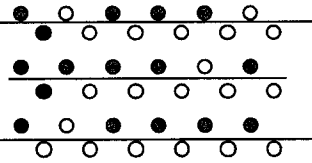	-0.34065 -0.34208
	Direct substitutions	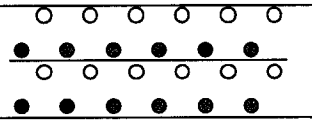	-0.34983 -0.34998

Table 4
Atom-by-atom energetics of two Pd atoms in NiTi

Configuration	M	Atom	E(strain) (eV/atom)	Glue	E(chemical) (eV/atom)	E(total) (eV/atom)	Net change with respect to NiTi (eV)
$Pd(Ti)Pd(Ti)_2$	2	Pd(Ti)	0.1300	1.2650	-0.1665	-0.0807	6.6738
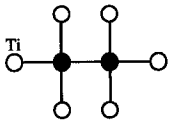	4	Ni_{11}	0.2886	0.6967	2.2783	1.8757	-3.3584
	8	Ni_{13}/Ni_{31}	0.2886	0.6967	2.8793	2.2944	-3.3672
	10	Ti_{23}/Ti_{32}	0.3433	1.3639	-2.8220	-3.5055	-0.8790
							-0.9308
$Pd(Ni)Pd(Ni)_2$	2	Pd(Ni)	0.1300	1.2650	0.6084	0.8996	-3.6314
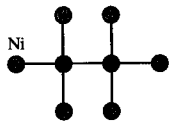	4	Ti_{11}	0.3433	1.3639	-2.3299	-2.8344	2.3328
	8	Ti_{13}/Ti_{31}	0.3433	1.3639	-2.5290	-3.1058	2.4944
	10	Ni_{23}/Ni_{32}	0.2886	0.6967	3.4812	2.7138	-0.0150
							1.1808

Table 5
Atom-by-atom energy analysis of four Pd atoms in NiTi

Configuration	M	Atom	E(strain) (eV/atom)	Glue	E(chemical) (eV/atom)	E(total) (eV/ atom)	Net change with respect to NiTi (eV)
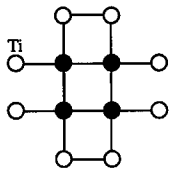	4	Pd(Ti)	0.1300	1.2650	-0.1682	-0.0828	13.3392
	2	Ni_{1111}	0.2886	0.6967	1.1237	1.0714	-3.2878
	8	Ni_{1313}	0.2886	0.6967	2.2783	1.8757	-6.7168
	8	Ni_{1333}	0.2886	0.6967	2.8793	2.2944	-3.3672
	16	Ti_{2333}	0.3433	1.3639	-2.8220	-3.5055	-1.4064
							-1.4390
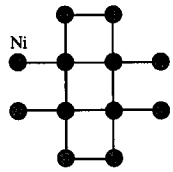	4	Pd(Ni)	0.1300	1.2650	0.6087	0.9000	-7.2612
	2	Ti_{1111}	0.3433	1.3639	-1.9963	-2.3793	2.0766
	8	Ti_{1313}	0.3433	1.3639	-2.3299	-2.8344	4.6656
	8	Ti_{1333}	0.3433	1.3639	-2.5290	-3.1058	2.4944
	16	Ni_{2333}	0.2886	0.6967	3.4812	2.7138	-0.0240
							1.9514

Table 6
Energies of formation of different eight Pd atom configurations in NiTi

Configuration	Energy of formation (eV/atom)	Lattice parameter (Å)	Configuration (see Fig. 3)
Eight Pd(Ti) atoms in a Ni(Ti,Pd) cell	-0.34598	3.01839	(a) Eight isolated Pd(Ni) atoms and (h) 2x2 patch
	-0.34659	3.01833	(g) Four Pd(Ni) coplanar dimers
	-0.34690	3.01830	(f) Two 4Pd(Ni) chains separated by a Ni row
	-0.34721	3.01827	(e) Eight Pd(Ni) chain
	-0.34779	3.01820	(d) Hexagonal Pd(Ni) patch
	-0.34779	3.01820	(c) Rectangular 8Pd(Ni) patch (4 consecutive dimers)
	-0.34838	3.01814	(b) B2 Pd(Ni)Ti precipitate
Eight Pd(Ni) atoms in a (Ni,Pd)Ti cell	-0.35120	3.01243	(a) Eight isolated Pd(Ti) atoms in different planes
	-0.35254	3.01368	(b) B2 NiPd(Ti) precipitate
	-0.35355	3.01355	(c) Rectangular 8Pd(Ti) patch (4 consecutive dimers)
	-0.35374	3.01353	(d) Hexagonal 8Pd(Ti) patch
	-0.35408	3.01349	(e) Eight Pd(Ti) chain
	-0.35445	3.01345	(f) Two 4Pd(Ti) chains separated by a Ti row
	-0.35479	3.01342	(g) Four Pd(Ti) coplanar dimers
	-0.35554	3.01334	(h) 2x2 patch

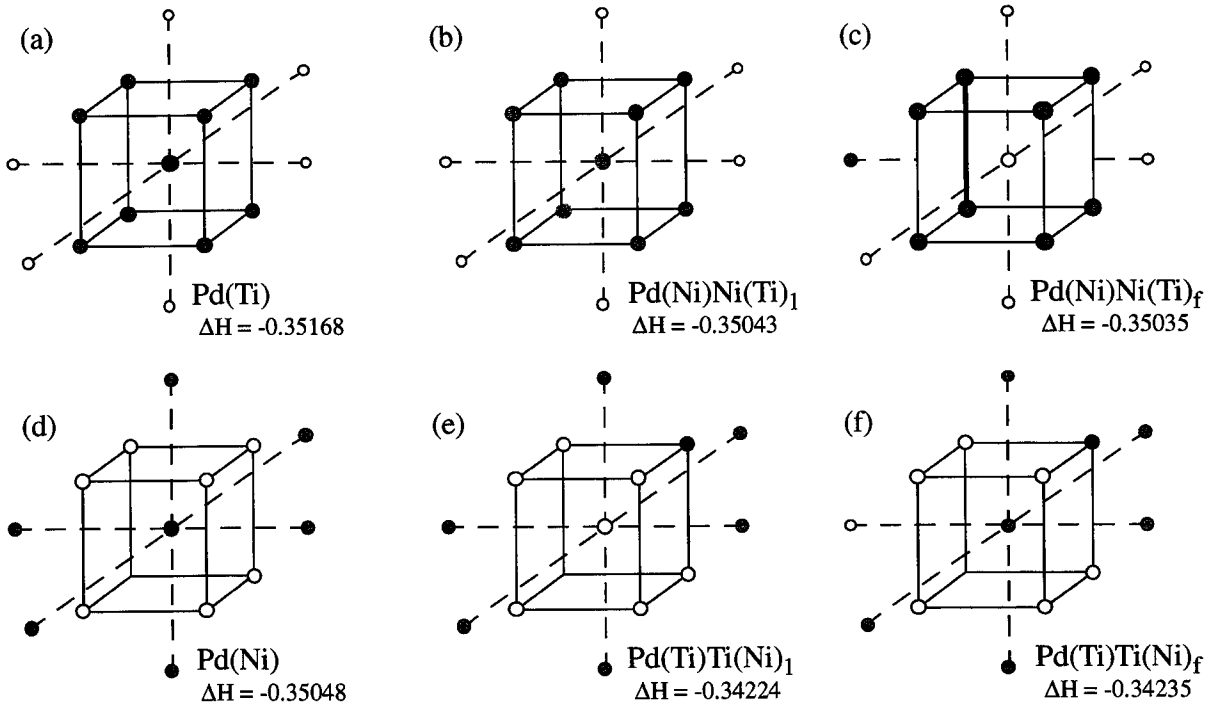
(a)
Pd(Ti)
ΔH = -0.35168
(b)
Pd(Ni)Ni(Ti)1
ΔH = -0.35043
(c)
Pd(Ni)Ni(Ti)f
ΔH = -0.35035
(d)
Pd(Ni)
ΔH = -0.35048
(e)
Pd(Ti)Ti(Ni)1
ΔH = -0.34224
(f)
Pd(Ti)Ti(Ni)f
ΔH = -0.34235

Fig. 1

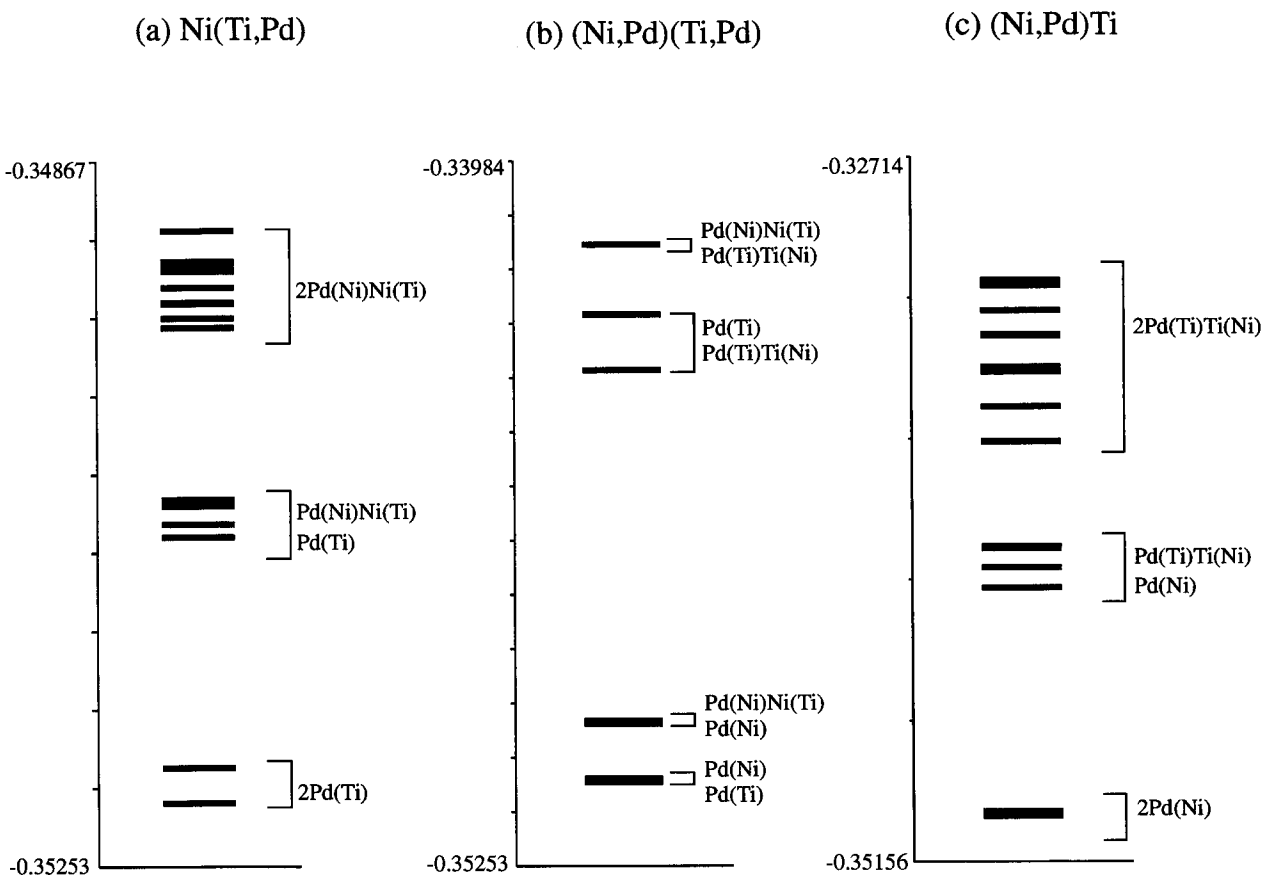
(a) Ni(Ti,Pd)
(b) (Ni,Pd)(Ti,Pd)
(c) (Ni,Pd)Ti
-0.34867
-0.35253
2Pd(Ni)Ni(Ti)
Pd(Ni)Ni(Ti)
Pd(Ti)
2Pd(Ti)
-0.33984
-0.35253
Pd(Ni)Ni(Ti)
Pd(Ti)Ti(Ni)
Pd(Ti)
Pd(Ti)Ti(Ni)
Pd(Ni)Ni(Ti)
Pd(Ni)
Pd(Ni)
Pd(Ti)
-0.32714
-0.35156
2Pd(Ti)Ti(Ni)
Pd(Ti)Ti(Ni)
Pd(Ni)
2Pd(Ni)

Fig. 2

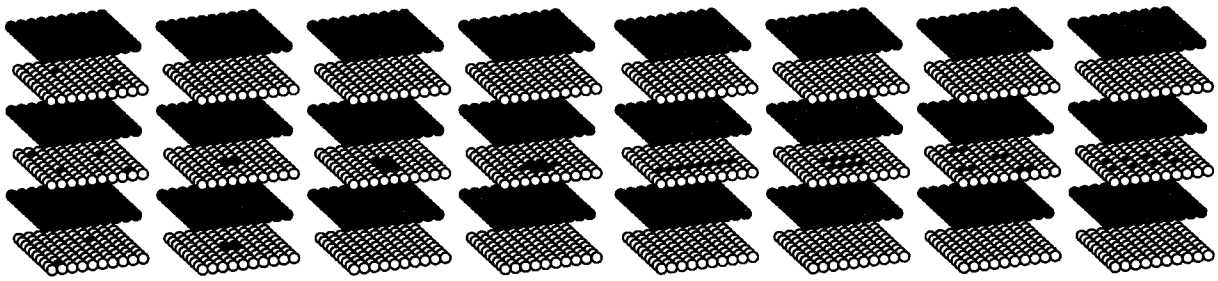

Fig. 3

(a) $Ni_{50}Ti_{49}Pd_1$

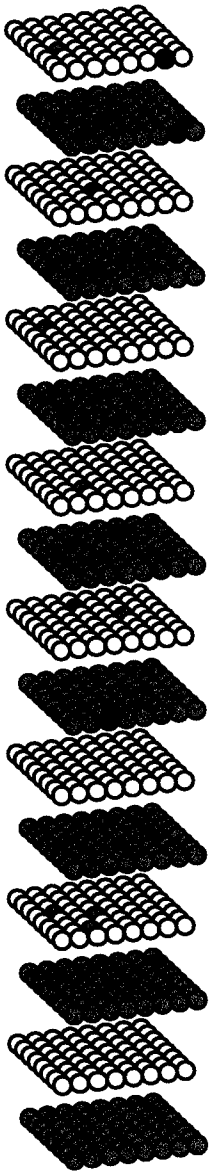

(b) $Ni_{50}Ti_{45}Pd_5$

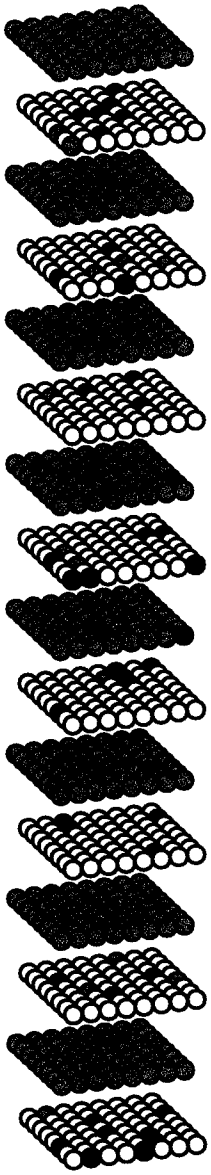

(c) $Ni_{50}Ti_{40}Pd_{10}$

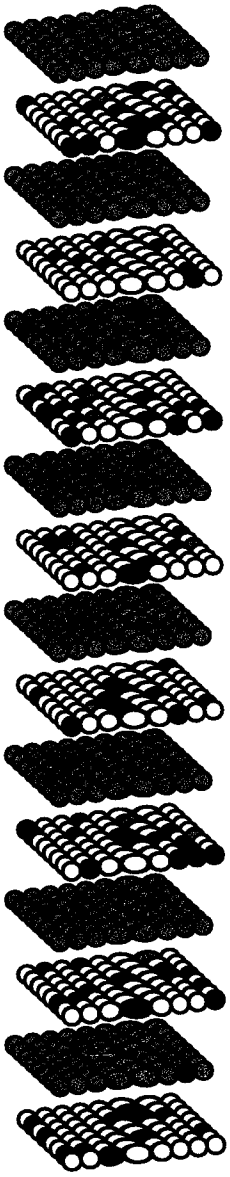

Fig. 4

(a) $Ni_{50}Ti_{49}Pd_1$ (b) $Ni_{50}Ti_{45}Pd_5$ (c) $Ni_{50}Ti_{40}Pd_{10}$

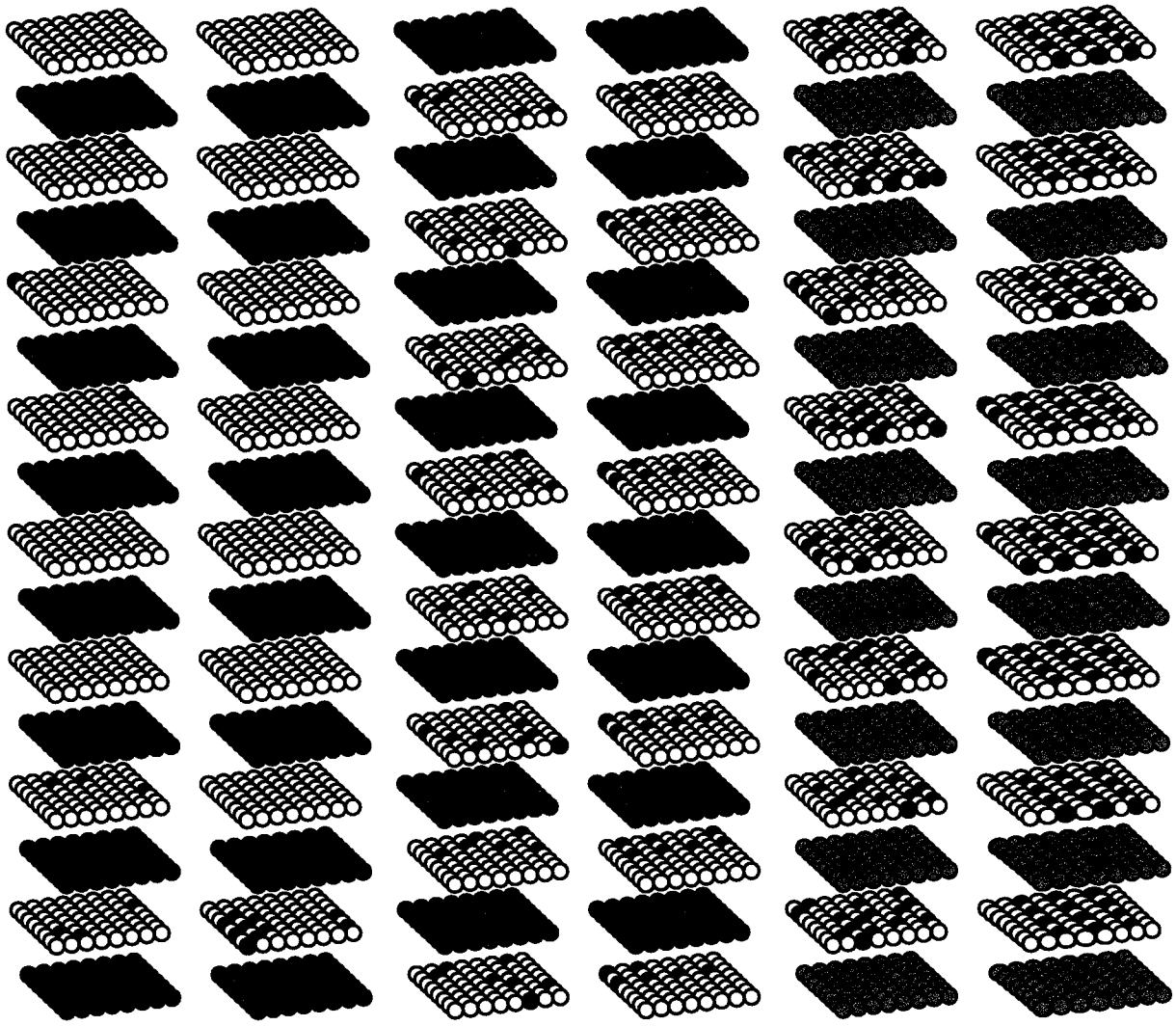

Fig. 5

(a) $Ni_{49}Ti_{50}Pd_1$

(b) $Ni_{45}Ti_{50}Pd_5$

(c) $Ni_{40}Ti_{50}Pd_{10}$

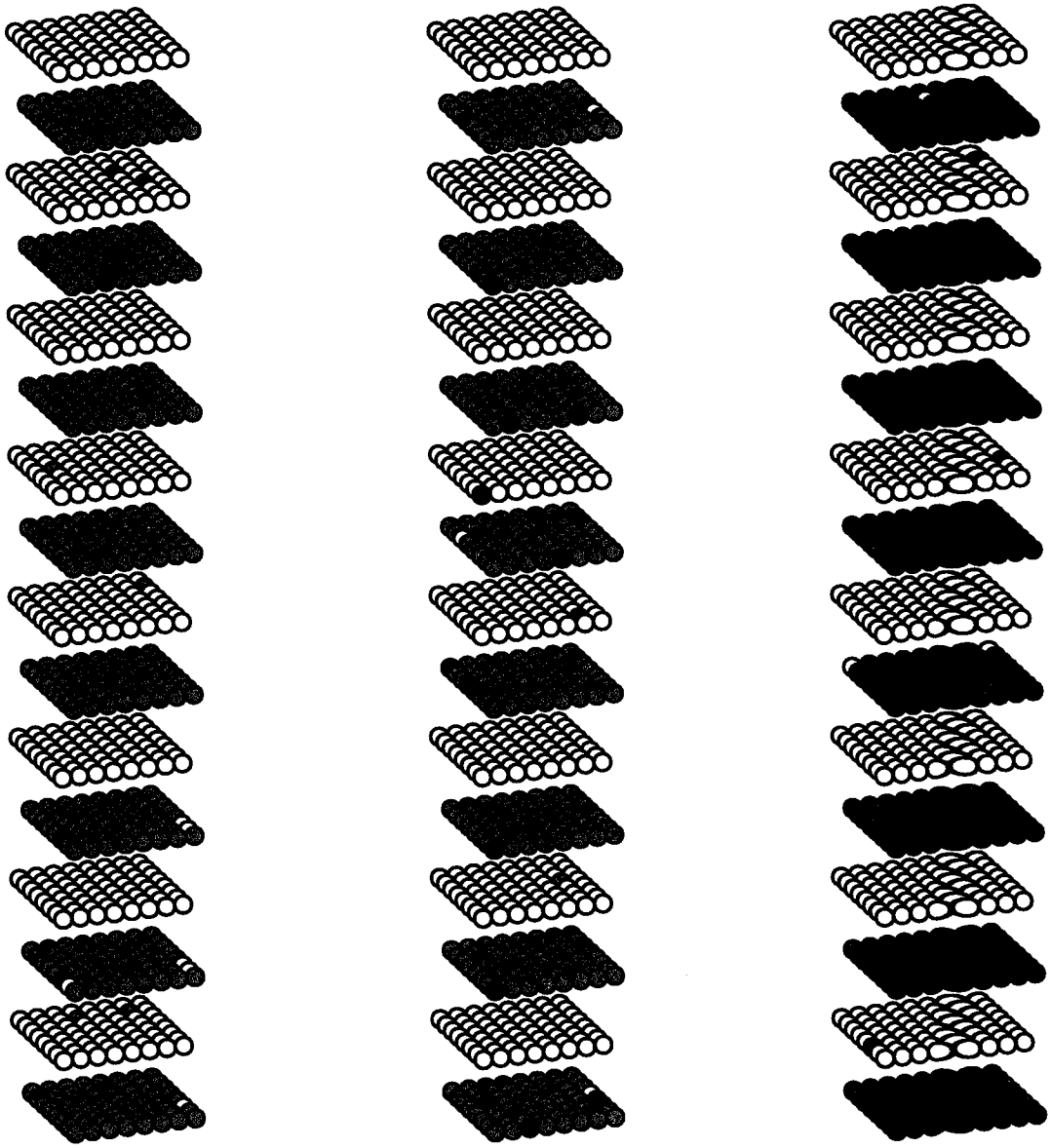

Fig. 6

(a) $Ni_{49}Ti_{50}Pd_1$ (b) $Ni_{45}Ti_{50}Pd_5$ (c) $Ni_{40}Ti_{50}Pd_{10}$

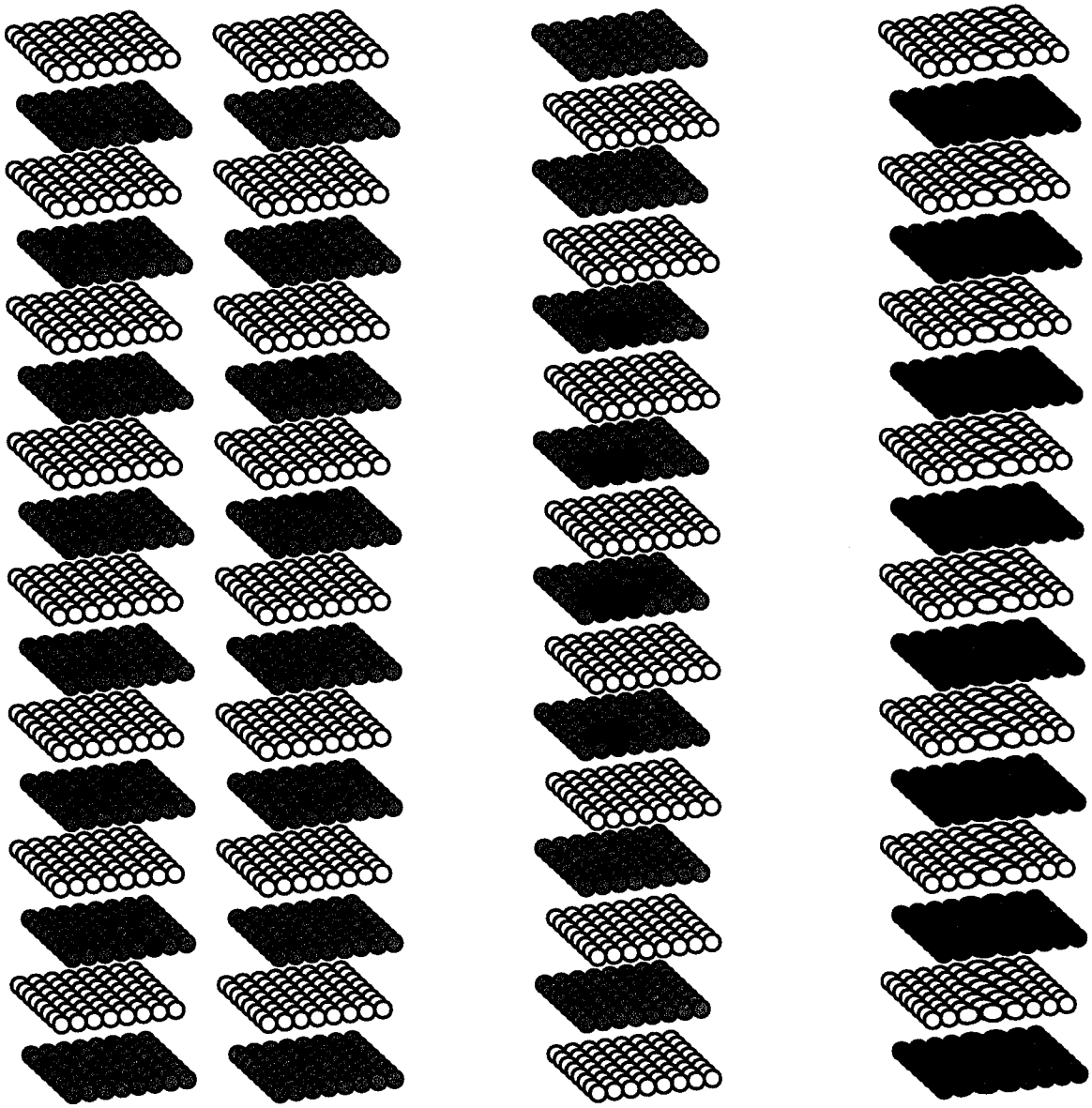

T = 1000 K T = 1 K

Fig. 7

(a) $Ni_{49}Ti_{49}Pd_2$

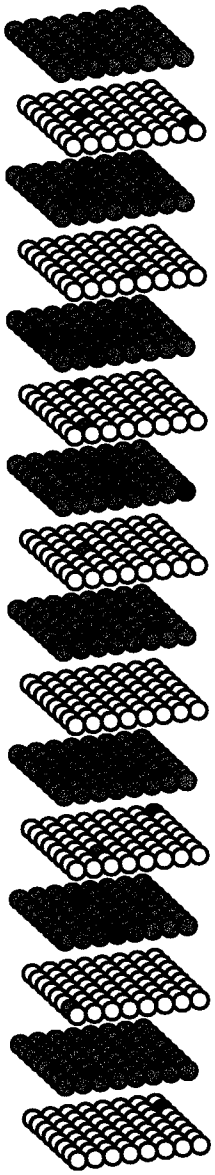

(b) $Ni_{45}Ti_{45}Pd_{10}$

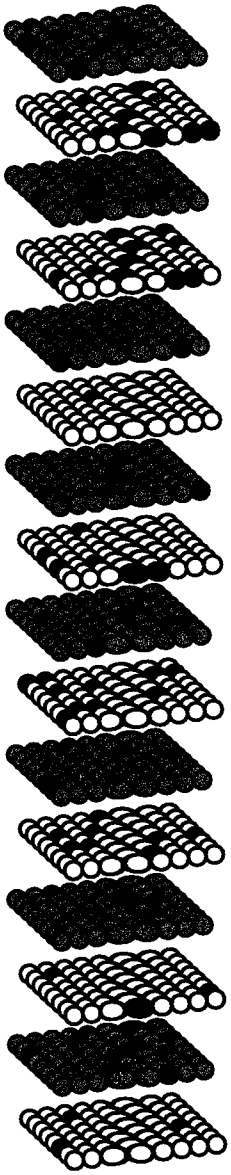

Fig. 8

(a) $Ni_{49}Ti_{49}Pd_2$

(b) $Ni_{45}Ti_{45}Pd_{10}$

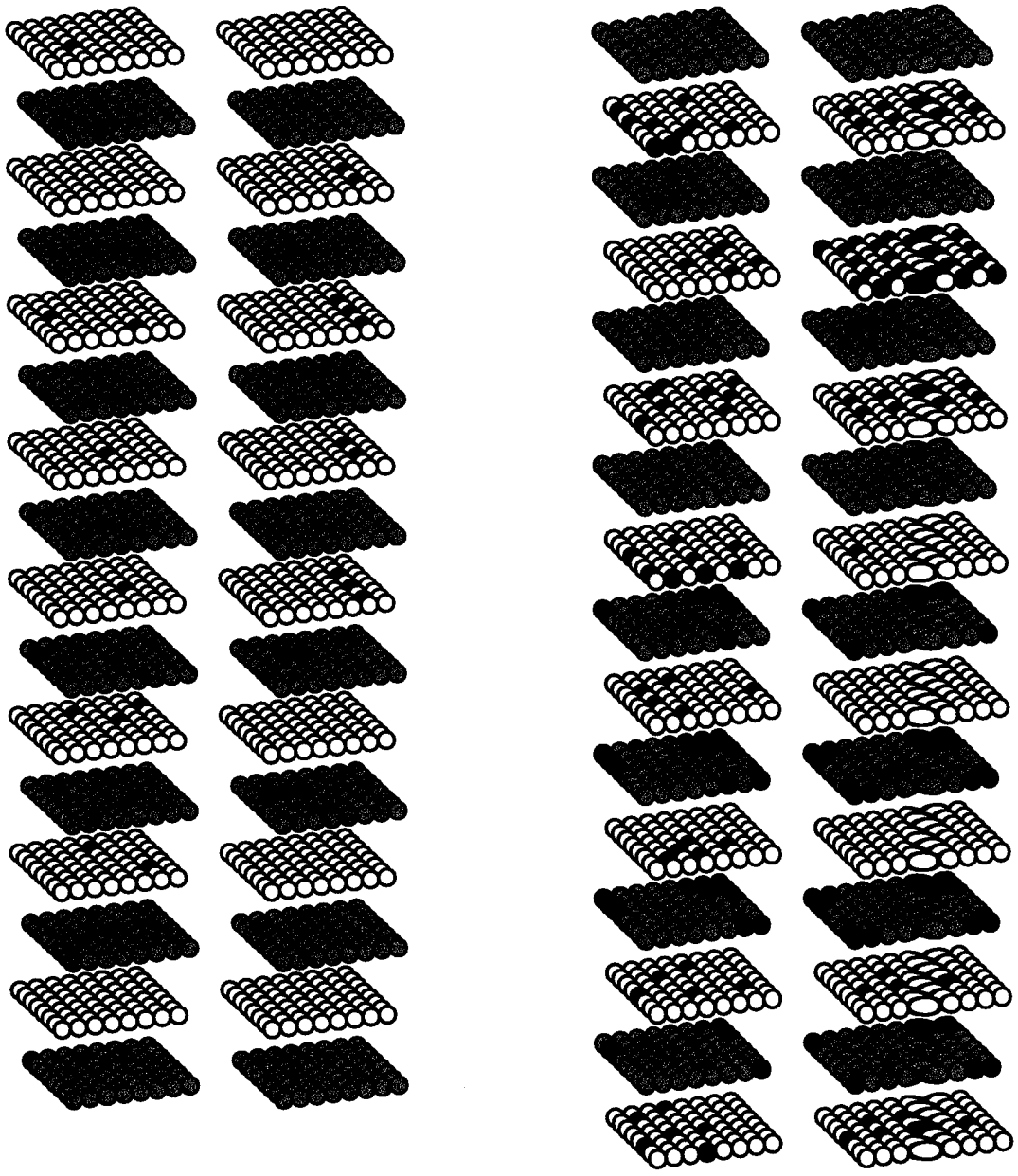

T = 1000 K T = 1 K

Fig. 9